

A Journal of the Gesellschaft Deutscher Chemiker

# Angewandte Chemie

GDCh

International Edition

www.angewandte.org

## Accepted Article

**Title:** A Top-Down Strategy to Realize Surface Reconstruction of Small-Sized Pt-Based Nanoparticles for Selective Hydrogenation

**Authors:** Xiaoqing Huang

This manuscript has been accepted after peer review and appears as an Accepted Article online prior to editing, proofing, and formal publication of the final Version of Record (VoR). This work is currently citable by using the Digital Object Identifier (DOI) given below. The VoR will be published online in Early View as soon as possible and may be different to this Accepted Article as a result of editing. Readers should obtain the VoR from the journal website shown below when it is published to ensure accuracy of information. The authors are responsible for the content of this Accepted Article.

**To be cited as:** *Angew. Chem. Int. Ed.* 10.1002/anie.202106459

**Link to VoR:** <https://doi.org/10.1002/anie.202106459>

# A Top-Down Strategy to Realize Surface Reconstruction of Small-Sized Pt-Based Nanoparticles for Selective Hydrogenation

Yu Jin,<sup>[a]</sup> Pengtang Wang,<sup>[a,b]</sup> Xinnan Mao,<sup>[c,d]</sup> Shangheng Liu,<sup>[a,b]</sup> Leigang Li,<sup>[a,b]</sup> Lu Wang,<sup>\*,[c]</sup> Qi Shao,<sup>[a]</sup> Yong Xu,<sup>\*,[d]</sup> Xiaoqing Huang<sup>\*,[a,b]</sup>

**Abstract:** Over the past decades, despite substantial efforts have been devoted to the modifications of Pt nanoparticles (NPs) for tailoring their selectivities for hydrogenation reactions, it is still lack of facile strategies for precisely regulating the surface properties of NPs, especially for those ones with small sizes. In this work, we propose a top-down thermal annealing strategy for tuning the surface properties of Pt-based NPs (~4 nm) without the occurrence of aggregation. Compare to conventional bottom-up methods, the present top-down strategy can precisely regulate the surface compositions of Pt-Cd NPs and other ternary Pt-Cd-M NPs (M = Fe, Ni, Co, Mn, and Sn). The optimized Pt-Cd NPs exhibit excellent selectivity toward phenylacetylene and 4-nitrostyrene hydrogenations with a styrene selectivity and 4-aminophenyl styrene selectivity of 95.2% and 94.5%, respectively. This work provides a general strategy for the surface reconstructions of Pt-based NPs, and promotes the fundamental researches on catalyst design for heterogeneous catalysis.

Noble-metals (e.g., Pt and Pd) have been widely used in hydrogenation reactions due to their excellent activities.<sup>[1]</sup> However, they suffer from the disadvantage of poor selectivity, and ideal catalysts for hydrogenations should be capable of simultaneously high activity, selectivity and stability.<sup>[2]</sup> Great efforts have been devoted to tailoring the selectivities for hydrogenations, such as compositing with promoters to suppress hydrogen adsorption and construct geometric effect to enable the hydrogenations at the specific groups of reactants.<sup>[1b, 3]</sup> Recently, composite NPs have emerged as new frontiers in selective hydrogenations because of the improved catalytic properties compared with single component.<sup>[4]</sup> Moreover, modifying noble metals with non-noble elements significantly reduces the cost of catalysts, and therefore attracts great interests.<sup>[5]</sup> For instance, Pd-Pb nanocubes (NCs),<sup>[6]</sup> Pd-Cd NCs,<sup>[2b]</sup> Pt-Zn NPs,<sup>[7]</sup> Pt-Fe nanowires (NWs),<sup>[8]</sup> Ru-Co

dumbbell-shaped nanostructures,<sup>[9]</sup> have been used as catalysts for selective hydrogenations. Despite great progress, the precise surface modifications of NPs, especially for NPs with small sizes, still remain great challenges, and two major concerns should be overcome: 1) it is lack of general protocols for obtaining and modifying small-sized NPs;<sup>[10]</sup> 2) the poor stability of small-sized NPs during pre-treatment and reaction limits their practical applications.<sup>[11]</sup>

Herein, we demonstrate a top-down thermal annealing strategy for surface reconstructions of Pt-Cd NPs (~4 nm). Compared to Pt, Cd atoms exhibit poorer stability against high temperatures, which can be pulled out from the inside and the surface of Pt-Cd NPs. Consequently, the surface compositions of Pt-Cd NPs can be precisely tailored by altering the annealing temperatures. Moreover, the reductive atmosphere during annealing leads to the variations of Pt<sup>2+</sup>/Pt<sup>0</sup> and Cd<sup>2+</sup>/Cd<sup>0</sup>. No aggregation of NPs occurred during thermal annealing even when the temperature was as high as 700 °C. Additionally, such strategy can be extended to other Pt-Cd-M NPs (M = Fe, Ni, Co, Mn, and Sn), being a versatile method for surface reconstruction. The optimized Pt-Cd NPs (Pt-Cd-650) exhibited excellent selectivities toward phenylacetylene and 4-nitrostyrene hydrogenations with a styrene selectivity and 4-aminophenyl styrene selectivity of 95.2% and 94.5%, respectively.

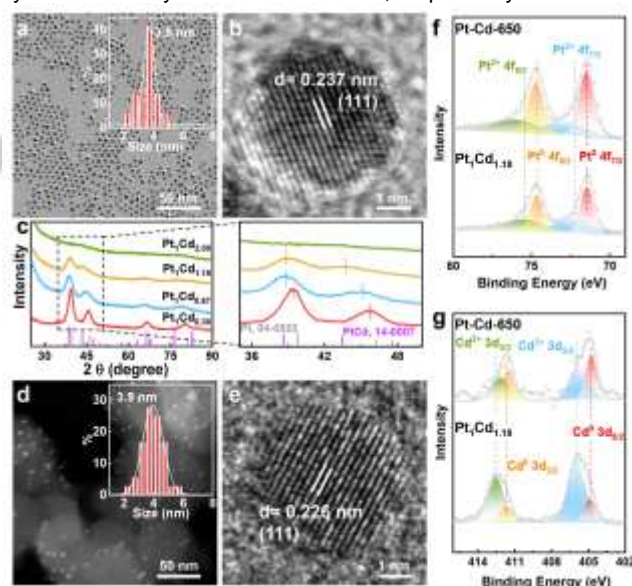


**Figure 1.** (a) TEM and (b) HRTEM images of pristine Pt<sub>1</sub>Cd<sub>1.18</sub> nanoparticles. (c) XRD patterns (left) and the enlarged patterns (right) of pristine Pt-Cd nanoparticles. (d) TEM and (e) HRTEM images of Pt-Cd-650. (f) Pt 4f and (g) Cd 3d XPS spectra of pristine Pt<sub>1</sub>Cd<sub>1.18</sub> NPs and Pt-Cd-650.

Pt-Cd NPs were prepared via a wet-chemical method (see details in **Supporting Information**). We took Pt<sub>1</sub>Cd<sub>1.18</sub> NP as an example. As shown in **Figure 1a**, monodispersed Pt-Cd NPs with mean size of ~3.8 nm were obtained. The lattice distance of 0.237 nm in the high-resolution transmission electron microscopy (HRTEM) image corresponded to Pt (111) facet, and the expansion of lattice distance was attributed to Cd

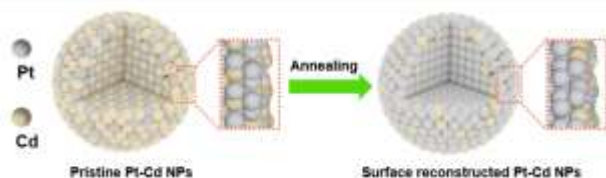
[a] Y. Jin, P. T. Wang, S. H. Liu, L. G. Li, Q. Shao, Prof. X. Q. Huang, College of Chemistry, Chemical Engineering and Materials Science, Soochow University, 215123, Suzhou, Jiangsu, China E-mail: hxq006@suda.edu.cn or hxq006@xmu.edu.cn

[b] State Key Laboratory of Physical Chemistry of Solid Surfaces, College of Chemistry and Chemical Engineering, Xiamen University, Xiamen, 361005, China

[c] X. Mao, Prof. L. Wang, Institute of Functional Nano & Soft Materials (FUNSOM), Jiangsu Key Laboratory for Carbon-Based Functional Materials & Devices, Soochow University, 215123, Suzhou, Jiangsu, China lwang@suda.edu.cn

[d] X. Mao, Prof. Y. Xu, Guangzhou Key Laboratory of Low-Dimensional Materials and Energy Storage Devices, Collaborative Innovation Center of Advanced Energy Materials, School of Materials and Energy, Guangdong University of Technology, 510006, Guangzhou, Guangdong, China yongxu@gdut.edu.cn Supporting information for this article is given via a link at the end of the document.

introduction (Figure 1b). Moreover, transmission electron microscope with spherical aberration (SA-TEM) measurement was performed to study the fine structure of Pt<sub>1</sub>Cd<sub>1.18</sub> NPs. It was found that the lattice distance of Pt (111) facet of Pt<sub>1</sub>Cd<sub>1.18</sub> NPs was slightly larger than 0.226 nm, further confirming the lattice expansion after Cd addition (Figure S1). The atomic ratio of Pt and Cd in Pt<sub>1</sub>Cd<sub>1.18</sub> NPs was 45.9/54.1 (determined by energy dispersive X-ray spectroscopy, EDS) (Figure S2 and Table S1). Other Pt-Cd NPs with different compositions were obtained by altering CdAc<sub>2</sub>·2H<sub>2</sub>O amounts during synthesis (Figure S3 and Table S1). In the absence of CdAc<sub>2</sub>·2H<sub>2</sub>O, the mean size of Pt NPs reached ~35 nm (Figure S3a), which greatly decreased to ~2.7 nm with the increased amounts of CdAc<sub>2</sub>·2H<sub>2</sub>O (Figure S3b-d). The negative shifts of the peak of (111) facet in X-Ray diffraction (XRD) patterns confirmed the lattice expansion after Cd introduction (Figure 1c).<sup>[12]</sup> Moreover, Pt-Cd NPs evolved to Pt-Cd intermetallic compound (PDF No.: 14-0007), and finally evolved to amorphous compound with the increase of Cd contents (Pt<sub>1</sub>Cd<sub>2.00</sub>, Figure 1c).<sup>[13]</sup>



**Scheme 1.** Schematic illustration for realizing surface reconstructed Pt-Cd NPs.

Pt<sub>1</sub>Cd<sub>1.18</sub> NPs were loaded on carbon support (VC-X72) and then annealed in H<sub>2</sub>/Ar (5 vol.% in Ar) for 1 h at 600, 650, and 700 °C, which were named as Pt-Cd-600, Pt-Cd-650, and Pt-Cd-700, respectively (Table S2). Considering the surface reconstructions were achieved through the escape of Cd atoms under high temperature,<sup>[14]</sup> Pt<sub>1</sub>Cd<sub>1.18</sub> NPs with a moderate Cd content were thus selected as the model for investigating the surface reconstructions (Scheme 1). It was found that the surface compositions of the annealed Pt-Cd NPs strongly depended on annealing temperatures. Pt-Cd-650 was selected as the example. TEM image showed that the mean size of Pt-Cd NPs was ~3.9 nm, which was slightly larger than that of Pt-Cd NPs before annealing (~3.8 nm) (Figure 1d). HRTEM image displayed the lattice distance of (111) facet was slightly smaller than that of pristine Pt<sub>1</sub>Cd<sub>1.18</sub> NPs, which was attributed to the Cd escape at 650 °C (Figure 1e). Moreover, SA-TEM image of Pt-Cd-650 showed that the lattice of Pt (111) facet at the near shell position was slightly larger than that at the core position, which was attributed to the migration of Cd atoms under high temperature annealing (Figure S4). The positive shifts of peaks in the XRD patterns of annealed NPs further confirmed the lattice contraction after Cd escape (Figure S5). The inductively coupled plasma-atomic emission spectrometry (ICP-AES) measurement results implied that the atomic ratios of Pt in the annealed Pt-Cd NPs gradually increased with temperatures for annealing (Table S2). Moreover, the surface properties of the annealed Pt-Cd NPs were studied by X-ray photoelectron spectroscopy (XPS) measurement.<sup>[15]</sup> The surface atomic percentage of Pt increased from 72.9% to 91.8% when the annealing temperature was increased from 600 to 700 °C (Figure 1f, g and Table S2). On the other hand, the Pt contents increased from 80.0% to 98.0% (by ICP-AES) with the increased annealing temperature from 600 to 700 °C (Table S2). The above results suggest that the migration (from inside to surface)

and evaporation (escape from surface) of Cd atoms simultaneously occurred during the annealing process. Additionally, no obvious aggregation of Pt-Cd NPs was observed even when the annealing temperature was as high as 700 °C (Figure S6), indicating that such annealing process could serve as an efficient strategy for the surface reconstruction of Pt-based NPs.

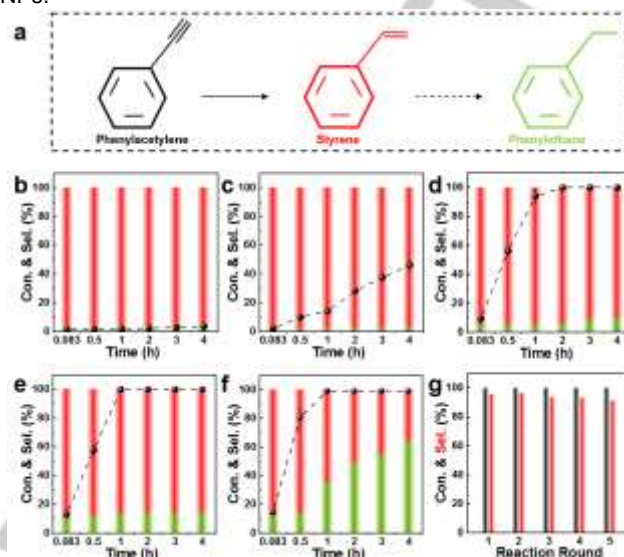


**Figure 2.** Catalytic performance for phenylacetylene hydrogenation over the annealed Pt-Cd nanoparticles. (a) Schematic of phenylacetylene hydrogenation reaction. Phenylacetylene hydrogenation over Pt<sub>1</sub>Cd<sub>1.18</sub> (b), Pt-Cd-600 (c), Pt-Cd-650 (d), Pt-Cd-700 (e), and Pt<sub>1</sub>Cd<sub>0.18</sub>-BM (f). (g) Phenylacetylene conversion and styrene selectivity in five consecutive rounds over Pt-Cd-650. Black dots in (b)-(f): phenylacetylene conversion.

To investigate the effects of surface reconstruction on catalytic performance, the annealed Pt-Cd NPs were used as catalyst for phenylacetylene hydrogenation (Figure 2a), and pristine Pt<sub>1</sub>Cd<sub>0.30</sub>, Pt<sub>1</sub>Cd<sub>0.67</sub>, Pt<sub>1</sub>Cd<sub>1.18</sub>, Pt<sub>1</sub>Cd<sub>2.00</sub>, and Pt<sub>1</sub>Cd<sub>0.18</sub>-BM with a similar surface Pt/Cd ratio to Pt-Cd-650 (Figure S7) were used as references. Prior to catalytic test, infrared spectroscopy (IR) measurement was performed to check the residual ligands on the surface of NPs. No peaks corresponding to oleylamine, borane morpholine and glucose were observed in the IR spectra of Pt<sub>1</sub>Cd<sub>1.18</sub>, and Pt<sub>1</sub>Cd<sub>0.18</sub>-BM (Figure S8), indicating that most of the surface ligands were removed. For catalysis, Pt<sub>1</sub>Cd<sub>0.67</sub>, Pt<sub>1</sub>Cd<sub>1.18</sub>, and Pt<sub>1</sub>Cd<sub>2.00</sub> with high content of Cd displayed low activity towards phenylacetylene hydrogenation, despite the selectivity of styrene was over 90% (Figure 2b and S9). When Pt<sub>1</sub>Cd<sub>0.30</sub> was used as catalyst, the conversion of phenylacetylene was 87% after 20 min at a styrene selectivity of 88.4% (Figure S9). By contrast, the phenylacetylene conversion reached 46.1% at a styrene selectivity of 97.6% for Pt-Cd-600 (Figure 2c). When Pt-Cd-650 was used as catalyst, phenylacetylene was completely converted after 2 h with a styrene selectivity of 95.2% (Figure 2d). Compared to Pt-Cd-650, Pt-Cd-700 displayed a lower styrene selectivity of 86.2% at near-complete conversion (Figure 2e). To further elucidate the effects of surface reconstruction on phenylacetylene hydrogenation, Pt<sub>1</sub>Cd<sub>0.18</sub>-BM with similar composition and size to Pt-Cd-650 was used as catalyst for phenylacetylene hydrogenation. Compared to Pt-Cd-650, Pt<sub>1</sub>Cd<sub>0.18</sub>-BM exhibited higher phenylacetylene conversion but much lower styrene selectivity (Figure 2f). Moreover, the styrene selectivity rapidly decreased with the reaction time, which was caused by the overhydrogenation of styrene. The aforementioned results indicated

that the surface reconstruction of Pt-Cd NPs strongly influenced the catalytic performance in terms of activity and selectivity.

Afterwards, the stability of Pt-Cd-650 was evaluated in five consecutive rounds for phenylacetylene hydrogenation. In addition to the maintenances of morphology and structure for the spent Pt-Cd-650 (**Figure S10**), no obvious decays in the activity and selectivity implied that Pt-Cd-650 could serve as highly stable a catalyst for phenylacetylene hydrogenation (**Figure 2g** and **Table S3**). Additionally, Pt-Cd-650 and Pt<sub>1</sub>Cd<sub>0.18</sub>-BM were used as catalysts for 4-nitrostyrene hydrogenation to further study the effects of surface reconstruction on selective hydrogenations (**Figure S11a**). Pt-Cd-650 displayed a nearly complete conversion at a 4-aminophenyl styrene selectivity of 94.5%, while the selectivities to 4-ethyl aniline and 4-ethyl nitrobenzene were 3% and 2.5%, respectively (**Figure S11b**). In sharp contrast, 4-nitrostyrene was completely converted into 4-ethyl aniline over Pt<sub>1</sub>Cd<sub>0.18</sub>-BM (**Figure S11c**). Compared to other reported catalysts, Pt-Cd-650 exhibited much higher activity and/or selectivity for the selective hydrogenation of 4-nitrostyrene (**Table S4**).

Detailed characterizations were performed for Pt<sub>1</sub>Cd<sub>0.18</sub>-BM to understand the significance of surface reconstruction on catalytic performance. TEM image showed that the mean size of Pt<sub>1</sub>Cd<sub>0.18</sub>-BM was ~3.9 nm (**Figure 3a**), and Pt<sub>1</sub>Cd<sub>0.18</sub>-BM had a similar composition to Pt-Cd-650 (**Figure S12** and **Table S5**). Results from XPS measurement displayed that the surface ratios of Cd/Pt for Pt-Cd-650 and Pt<sub>1</sub>Cd<sub>0.18</sub>-BM were 16.5/83.5 and 10.9/89.1, respectively (**Figure 3b, c** and **Table S2**). Compared to Pt-Cd-650, the peaks in the XRD pattern of Pt<sub>1</sub>Cd<sub>0.18</sub>-BM negatively shifted by 0.43°, indicating the lattice contraction in Pt-Cd-650 (**Figure S13**). Correspondingly, the lattice distance for Pt-Cd-650 was 0.226 nm, which was slightly smaller than that for Pt<sub>1</sub>Cd<sub>0.18</sub>-BM (0.229 nm) (**Figure 3d**). Moreover, electrochemical activity specific surface area (ECSA) measurement without activation treatment was used to study the surface properties of Pt-Cd-650 and Pt<sub>1</sub>Cd<sub>0.18</sub>-BM. The ECSA value of Pt-Cd-650 was 14.7 m<sup>2</sup> g<sub>pt</sub><sup>-1</sup>, which was much smaller than that of Pt<sub>1</sub>Cd<sub>0.18</sub>-BM (27.8 m<sup>2</sup> g<sub>pt</sub><sup>-1</sup>), suggesting the Pt-rich surface of Pt<sub>1</sub>Cd<sub>0.18</sub>-BM (**Figure 3e**). Compared to Pt-Cd-650, the larger CO stripping area for Pt<sub>1</sub>Cd<sub>0.18</sub>-BM further confirmed the Pt-rich surface of Pt<sub>1</sub>Cd<sub>0.18</sub>-BM (**Figure S14**). Pt-rich surface may lead to strong adsorptions of reactants and consequential high activity and low selectivity. Compared to Pt-Cd-650, the *d*-band center for Pt<sub>1</sub>Cd<sub>0.18</sub>-BM was more close to Fermi level, suggesting the weaker absorptions of reactants on Pt-Cd-650 (**Figure 3f**).<sup>[16]</sup>

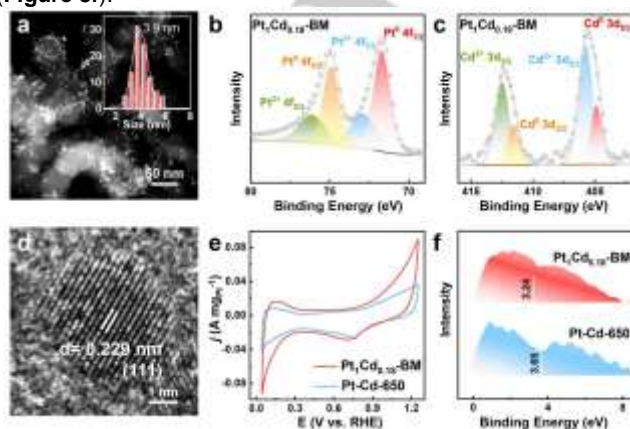


**Figure 3.** (a) TEM image and size distribution (inset of a), (b) Pt 4f and (c) Cd 3d XPS spectra and (d) HRTEM image of Pt<sub>1</sub>Cd<sub>0.18</sub>-BM. (e) CV curves with 50 mV s<sup>-1</sup> scanning speed for Pt-Cd-650 and Pt<sub>1</sub>Cd<sub>0.18</sub>-BM in 0.1 M HClO<sub>4</sub> solution. (f) Surface valence bands for Pt-Cd-650 and Pt<sub>1</sub>Cd<sub>0.18</sub>-BM.

Considering the surface reconstruction might lead to the variations of Pt<sup>2+</sup>/Pt<sup>0</sup> and Cd<sup>2+</sup>/Cd<sup>0</sup> ratios, and further influenced the surface electronic properties of NPs.<sup>[32-34]</sup> Control experiments were performed to investigate the variations of Pt<sup>2+</sup>/Pt<sup>0</sup> and Cd<sup>2+</sup>/Cd<sup>0</sup> ratios on the surface of Pt-Cd NPs. We selected Pt<sub>1</sub>Cd<sub>0.18</sub>-BM as a model and annealed it in H<sub>2</sub>/Ar (5 vol.% in Ar) at 250 °C for 1 h (named as Pt<sub>1</sub>Cd<sub>0.18</sub>-BM-250). XPS fittings indicated that the surface ratio of Pt/Cd in Pt<sub>1</sub>Cd<sub>0.18</sub>-BM (89.3/10.7) was close to that of Pt<sub>1</sub>Cd<sub>0.18</sub>-BM-250 (89.1/10.9) (**Figure S15** and **Table S6**), indicating that Pt<sub>1</sub>Cd<sub>0.18</sub>-BM did not experience surface reconstruction at 250 °C. However, the ratios of Pt<sup>2+</sup>/Pt<sup>0</sup> and Cd<sup>2+</sup>/Cd<sup>0</sup> significantly varied after annealing in H<sub>2</sub>/Ar (5 vol.% in Ar) at 250 °C for 1 h. In particular, the ratios of Pt<sup>2+</sup>/Pt<sup>0</sup> and Cd<sup>2+</sup>/Cd<sup>0</sup> for Pt<sub>1</sub>Cd<sub>0.18</sub>-BM were 42.3/57.7 and 71.5/28.5, respectively, which decreased to 38.9/61.1 and 42.6/57.4 in Pt<sub>1</sub>Cd<sub>0.18</sub>-BM-250 (**Table S6**). For phenylacetylene hydrogenation, Pt<sub>1</sub>Cd<sub>0.18</sub>-BM-250 displayed slight higher styrene selectivity (89.0%) than that of Pt<sub>1</sub>Cd<sub>0.18</sub>-BM (83.0%) at a phenylacetylene conversion of ~85% (**Figure S16**). For 4-nitrostyrene hydrogenation, Pt<sub>1</sub>Cd<sub>0.18</sub>-BM-250 exhibited obviously-enhanced 4-aminophenyl styrene selectivity compared to Pt<sub>1</sub>Cd<sub>0.18</sub>-BM (**Figure S17**). The aforementioned results implied that the selectivity was related to the variations of Pt<sup>2+</sup>/Pt<sup>0</sup> and Cd<sup>2+</sup>/Cd<sup>0</sup> ratios on the surface after surface reconstruction.

Density functional theory (DFT) calculations were performed to gain deep insights of surface reconstruction on phenylacetylene hydrogenation. Pt (111) surface was chosen as the initial structure to represent the energetically stable facet. Pt-Cd NPs were constructed by replacing Pt with Cd atoms at the subsurface sites and surface sites. To simulate the different reconstructed Pt-Cd surfaces under different temperatures, the compositions of Pt and Cd at the surface and subsurface were changed. Considering the styrene selectivity is determined by the desorption ability of styrene, and we thus optimized the adsorption configurations of styrene on different Pt-Cd surfaces to estimate the styrene selectivity. On Pt (111) surface, the styrene possessed a flat adsorption configuration (**Figure 4a**) and the adsorption energy of styrene was -3.95 eV, indicating that styrene was difficult to desorb from the surface and. On the pristine Pt-Cd surface, the Cd atoms were mostly distributed in the inner instead of surface (**Figure 4b**), and the adsorption energy of styrene was -2.25 eV, which was smaller than that on Pt (111) surface. After annealing, the Pt-Cd surface was reconstructed and more Cd atoms diffused into the surface (**Figure 4**). The adsorption energy of styrene dramatically decreased to -1.27 eV with the tilted adsorption configuration. The relatively weak interaction between styrene and the reconstructed Pt-Cd surface facilitates styrene desorption and thus suppresses the over-hydrogenation of styrene. More Cd atoms escaped from the surface with the increased annealing temperature, and the adsorption energy of styrene significantly increased to -3.42 eV due to the increasing surface atomic percentage of Pt, resulting in the significant decrease of styrene selectivity (**Figure 4d**). The projected density of states (PDOS) further demonstrated the interaction between styrene and Pt-Cd surface (**Figure 4e-h**). The hybridization between C 2p in styrene and Pt 5d orbitals on pure Pt surface located in the deep

and wide energies, while the hybridization peaks obviously moved near to the Fermi level for the surface reconstructed Pt-Cd with more Cd atoms on the surface, suggesting a relatively weak interaction. Thus, by controlling the reconstruction of Pt-Cd surface, a high selectivity towards styrene was achieved, which was well consistent with the experiments.

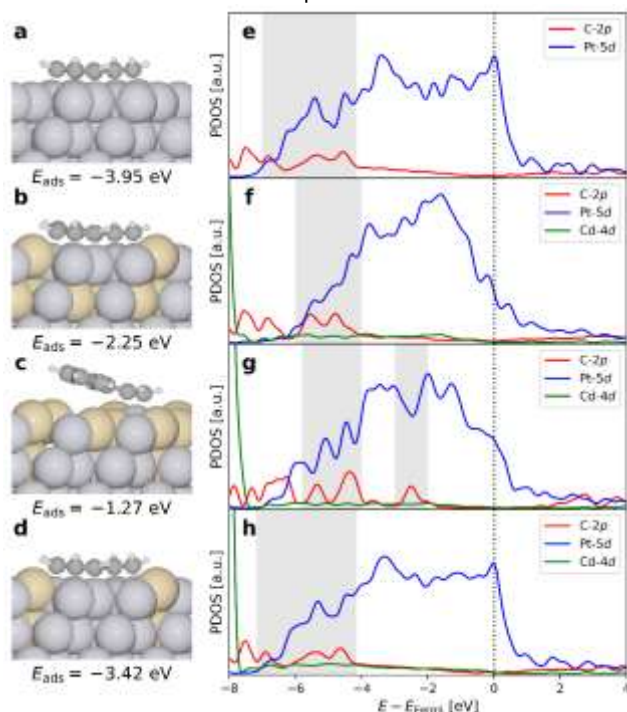


**Figure 4.** The adsorbed styrene configurations on (a) pure Pt and (b-d) different Pt-Cd surfaces with the calculated adsorption energies, and (e-h) the corresponding projected density of states (PDOS). The light grey ball and yellow ball represent Pt and Cd atoms, respectively. The dashed line indicates the Fermi level.

We synthesized ternary Pt-Cd-M NPs ( $M = \text{Ni, Fe, Co, Mn, and Sn}$ ) for surface reconstructions to demonstrate the universality of this strategy (Table S7). Pt-Cd-M NPs were loaded on VC-X72 and subsequently annealed at 600 and 700 °C (named as Pt-Cd-M-600 and Pt-Cd-M-700, respectively) (Figures S18-20). We took Pt-Cd-Ni as an example. The mean size of pristine Pt-Cd-Ni NPs was ~4.2 nm (Figure S18a-c). After annealing at 600 °C, no obvious changes for the size of Pt-Cd-Ni NPs were observed (Figure S19). The surface ratio of Pt/Ni/Cd for pristine Pt-Cd-Ni NPs was 32.7/8.9/58.4, which evolved to 43.1/42.1/14.8 and 61.7/34.2/4.1 after annealing at 600 and 700 °C, respectively (Tables S8 and S9). Compared to the pristine Pt-Cd-M NPs, the lattice contractions in the HRTEM images of annealed Pt-Cd-M NPs indicated the migration and escape of Cd atoms under high temperatures (Figures S20 and Table S9). Correspondingly, the lattice distance of (111) facet for pristine Pt-Cd-Ni NPs was 0.228 nm (Figure S28c), which decreased to 0.222 nm after annealing at 600 °C (Figure S20b). Similar results were observed for other Pt-Cd-M NPs ( $M = \text{Fe, Co, Mn, and Sn}$ ) (Figure S20s), indicating the universality of this strategy for surface reconstruction.

In summary, we have demonstrated a top-down thermal annealing strategy for surface reconstructions of Pt-based NPs. Such strategy solely led to the variations in the surface compositions without aggregation of Pt-based NPs even when the annealing temperature was as high as 700 °C. The universality of this strategy was further validated by the surface

reconstructions of other Pt-Cd-M NPs ( $M = \text{Fe, Ni, Co, Mn, and Sn}$ ). We believe this work not only provides a unique strategy for the surface reconstructions of Pt-based NPs, but also sheds new lights on designing highly selective catalysts for hydrogenation.

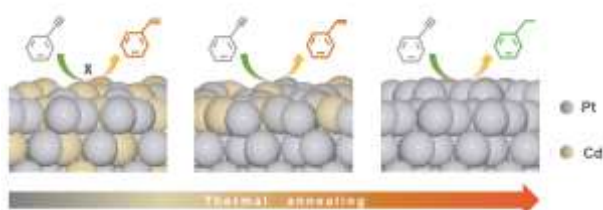
## Acknowledgements

This work was financially supported by Ministry of Science and Technology (2017YFA0208200, 2016YFA0204100), the National Natural Science Foundation of China (22025108, 51802206), Natural Science Foundation of Jiangsu Province (BK20180846), the Priority Academic Program Development of Jiangsu Higher Education Institutions (PAPD), the Project of Scientific and Technologic Infrastructure of Suzhou (SZS201905), and Guangdong Provincial Key Laboratory of Energy Materials for Electric Power (No. 2018B030322001). Yong Xu acknowledges the start-up supports from Guangdong University of Technology. Yu Jin, Pengtang Wang and Xinnan Mao contributed equally to this work.

**Keywords:** Platinum • Cadmium • Top-Down • Surface reconstruction • Hydrogenation

- [1] B. Wu, H. Huang, J. Yang, N. Zheng, G. Fu, *Angew. Chem. Int. Ed.* **2012**, *51*, 3440-3443.
- [2] G. Chen, C. Xu, X. Huang, J. Ye, L. Gu, G. Li, Z. Tang, B. Wu, H. Yang, Z. Zhao, Z. Zhou, G. Fu, N. Zheng, *Nat. Mater.* **2016**, *15*, 564-569.
- [3] S. T. Marshall, M. O. Brien, B. Oetter, A. Corpuz, R. M. Richards, D. K. Schwartz, J. W. Medlin, *Nat. Mater.* **2010**, *9*, 853-858.
- [4] F. Meemken, A. Baiker, *Chem. Rev.* **2017**, *117*, 11522-11569.
- [5] J. Zhang, W. Xu, L. Xu, Q. Shao, X. Huang, *Chem. Mater.* **2018**, *30*, 6338-6345.
- [6] Y. Feng, W. Xu, B. Huang, Q. Shao, L. Xu, S. Yang, X. Huang, *J. Am. Chem. Soc.* **2020**, *142*, 962-972.
- [7] H. Wang, X.-K. Gu, X. Zheng, H. Pan, J. Zhu, S. Chen, L. Cao, W.-X. Li, J. Lu, *Sci. Adv.* **2019**, *5*, eaat6413-6421.
- [8] H. Wang, J. Lu, *Chin. J. Chem.* **2020**, *38*, 1422-1444.
- [9] Y. Xu, L. Chen, X. Wang, W. Yao, Q. Zhang, *Nanoscale* **2015**, *7*, 10559-10583.
- [10] M. D. Marcinkowski, M. T. Darby, J. Liu, J. M. Wimple, F. R. Lucci, S. Lee, A. Michaelides, M. Flytzani-Stephanopoulos, M. Stamatakis, E. C. H. Sykes, *Nat. Chem.* **2018**, *10*, 325-332.
- [11] F. Tao, *Chem. Soc. Rev.* **2012**, *41*, 7977-7979.
- [12] L. Luo, M. Wang, Y. Cui, Z. Chen, J. Wu, Y. Cao, J. Luo, Y. Dai, W. X. Li, J. Bao, J. Zeng, *Angew. Chem. Int. Ed.* **2020**, *59*, 14434-14442.
- [13] W. Niu, Y. Gao, W. Zhang, N. Yan, X. Lu, *Angew. Chem. Int. Ed.* **2015**, *54*, 8271-8274.
- [14] A. Han, J. Zhang, W. Sun, W. Chen, S. Zhang, Y. Han, Q. Feng, L. Zheng, L. Gu, C. Chen, Q. Peng, D. Wang, Y. Li, *Nat. Commun.* **2019**, *10*, 3787-3794.
- [15] S. Bai, L. Bu, Q. Shao, X. Zhu, X. Huang, *J. Am. Chem. Soc.* **2018**, *140*, 8384-8387.
- [16] J. Mao, W. Chen, W. Sun, Z. Chen, J. Pei, D. He, C. Lv, D. Wang, Y. Li, *Angew. Chem. Int. Ed.* **2017**, *56*, 11971-11975.
- [16] S. Bai, L. Bu, Q. Shao, X. Zhu, X. Huang, *J. Am. Chem. Soc.* **2018**, *140*, 8384-8387.
- [17] L. Zhang, F. Hou, Y. Tan, *Chem. Commun.* **2012**, *48*, 7152-7154.
- [18] C. Wang, D. P. Chen, X. Sang, R. R. Unocic, S. E. Skrabalak, *ACS Nano* **2016**, *10*, 6345-6353.
- [19] C. E. Carlton, S. Chen, P. J. Ferreira, L. F. Allard, S. H. Yang, *J. Phys. Chem. Lett.* **2012**, *3*, 161-166.
- [20] S. Chen, Z. Wei, X. Qi, L. Dong, Y. G. Guo, L. Wan, Z. Shao, L. Li, *J. Am. Chem. Soc.* **2012**, *134*, 13252-13255.
- [21] M. Bao, X. Chen, S. Hu, L. Zhang, Y. Li, C. Carraro, R. Maboudian, W. Wei, Y. Zhang, S. Liu, *J. Mater. Chem. A* **2020**, *8*, 21327-21338.
- [22] P. Wang, Q. Shao, X. Cui, X. Zhu, X. Huang, *Adv. Funct. Mater.* **2018**, *28*, 1705918-1705928.

- [23] Q. Yun, Q. Lu, C. Li, B. Chen, Q. Zhang, Q. He, Z. Hu, Z. Zhang, Y. Ge, N. Yang, J. Ge, Y. B. He, L. Gu, H. Zhang, *ACS Nano* **2019**, *13*, 14329-14336.
- [24] J. S. Kim, I. Park, E. S. Jeong, K. Jin, W. M. Seong, G. Yoon, H. Kim, B. Kim, K. T. Nam, K. Kang, *Adv. Mater.* **2017**, *29*, 1606893-1606900.
- [25] A. V. Zadesenets, A. B. Venediktov, Y. V. Shubin, S. V. Korenev, *Russ. J. Inorg. Chem.* **2007**, *52*, 500-504.
- [26] F. Gao, Z. Xu, H. Zhao, *Proc. Combust. Inst.* **2020**. <https://doi.org/10.1016/j.proci.2020.06.330>.
- [27] O. Tukhlibaev, A. T. Tursunov, É. É. Khalilov, *Opt. Spectrosc.* **2001**, *91*, 571-575.
- [28] G. Zha, C. Yang, Y. Wang, X. Guo, W. Jiang, B. Yang, *Sep. Purif. Technol.* **2019**, *209*, 863-869.
- [29] Y. Zhu, L. Bu, Q. Shao, X. Huang, *ACS Catal.* **2020**, *10*, 3455-3461.
- [30] W. Wang, Z. Cao, K. Liu, J. Chen, Y. Wang, S. Xie, *Nano Lett.* **2017**, *17*, 7613-7619.
- [31] S. H. Han, H. M. Liu, P. Chen, J. X. Jiang, Y. Chen, *Adv. Energy Mater.* **2018**, *8*, 1801326-1801336.
- [32] Y. Bai, H. Huang, C. M. Wang, R. Long, Y. J. Xiong, *Mater. Chem. Front.* **2017**, *1*, 1951-1964.
- [33] Y. Long, J. Li, L. L. Wu, Q. S. Wang, Y. Liu, X. Wang, S. Y. Song, H. J. Zhang, *Nano Res.* **2019**, *12(4)*, 869-875.
- [34] F. Yang, S. P. Ding, H. B. Song, N. Yan, *Sci. China Mater.* **2020**, *63(6)*, 982-992.

**A Top-down Strategy for Surface Reconstruction**

Yu Jin, Pengtang Wang, Xinnan Mao, Shangheng Liu, Leigang Li, Lu Wang,\* Qi Shao, Yong Xu,\* Xiaoqing Huang\*

**A Top-Down Strategy to Realize Surface Reconstruction of Small-Sized Pt-Based Nanoparticles for Selective Hydrogenation**

A top-down thermal annealing strategy has been proposed for the precise surface reconstruction of Pt-based nanoparticles. The reconstructed nanoparticles display excellent stability at high temperature, yet serve as highly active and selective catalysts for the hydrogenations of phenylacetylene and 4-nitrostyrene.